Chemical Science

ROYAL SOCIETY OF CHEMISTRY

EDGE ARTICLE

View Article Online
View Journal | View Issue

Cite this: *Chem. Sci.*, 2023, **14**, 4319

All publication charges for this article have been paid for by the Royal Society of Chemistry

Received 4th February 2023
Accepted 19th March 2023

DOI: 10.1039/d3sc00642e

rsc.li/chemical-science

Molecular assembly of carbon nitride-based composite membranes for photocatalytic sterilization and wound healing†

Xiaoxiao Peng,‡[a] Jin Ma,‡[a] Zhixin Zhou,[a] Hong Yang,[a] Jingjing Chen,[a] Ran Chen,[a] Kaiqing Wu,[a] Guangcheng Xi,[c] Songqin Liu,[a] Yanfei Shen *[b] and Yuanjian Zhang *[a]

Polymeric carbon nitride (pCN) has attracted increasing interest as a metal-free photocatalyst because of its high efficiency in reactive oxygen species (ROS) generation. However, due to poor solubility, compounding pCN at the molecular level into more advanced nanocomposites remains a challenge. Herein, we report the dissolution of pCN in polyphosphoric acid (PPA) for the first time and fluid-phase assembly with carbon nanotubes (CNTs) into a flexible free-standing membrane. Mechanism and generality studies disclosed that the coordination of the acidity, viscosity, and adsorption energy of the solvents led to the successful dissolution of pCN. Interestingly, the pCN/CNTs molecular composite membrane exhibited not only superior mechanical properties and cycling performance as a result of strengthened π–π interfacial interaction, but also outstanding inactivation of *E. coli* and *S. aureus* in sterilization and wound healing for laboratory mice *via* photogenerated oxygen radicals. It would open a new era of pCN for biomedical applications in molecular composite membranes, beyond the traditional solar fuel applications in powders.

Introduction

Reactive oxygen species (ROS), chemical species formed upon incomplete reduction of oxygen,[1–6] mainly include hydroxyl radicals ($^{\bullet}OH$), superoxide ($^{\bullet}O_2^-$), singlet oxygen ($^1O_2$), and hydrogen peroxide (H_2O_2). These chemical species participate in phenomena that traverse all biological processes and exert versatile physiological and pathological functions in biological systems. Photocatalysis has always been recognized as a useful way to produce photogenerated ROS, which can act as strong oxidants to destroy harmful microorganisms[7–10] and play an essential role in disease therapy and environmental cleaning. Among them, polymeric carbon nitride (pCN),[11–20] a fine biocompatible[21,22] and visible light-responsive photocatalyst,[23–25] has been stimulated as a prospective candidate for photocatalytic bacterial disinfection for biomedical applications owing to the generation of ROS.[26–28] Nonetheless, most applications of pCN are still in the powder state,[29] and it is difficult to utilize the unique characteristics of pCN at the macroscale, such as the formation of free-standing membranes that are easy to handle and cycle with no loss of quality. Unfortunately, the particulate properties and insoluble nature[30–33] of pCN limit its combination with supplementary materials at the molecular level for advanced functional nanocomposites. It is foreseeable that realizing the dissolution of pCN will dramatically expand its scope of applications.

The dispersion and dissolution of pCN in liquids are exceedingly challenging, compared with those of other semiconductor-based nanomaterials and polymers, owing to the strong van der Waals forces between the 2D interlayers. Several pioneering efforts to exfoliate and disperse CN have been reported.[34–40] For example, pCN was first discovered to be dissolvable in concentrated sulfuric acid[41,42] ($pK_{a1} = -3.03$) and methyl sulfonic acid[43] ($pK_a = -1.61$, Table S1†) because of protonation and intercalation. Carbon nitride derivatives, such as poly(triazine imide) (PTI–LiBr)[44] and K, Na-poly(heptazine imide)[32] (PHI), can be dissolved in dimethyl sulfoxide (DMSO) or dispersed in water as colloidal nanoparticles. For practical nanocomposite applications, pristine pCN dissolution still suffers from limited solvent types and solubilities. Moreover, strong oxidizing acids are highly corrosive with complicated application procedures and/or incompatible with other processes, which impedes their popularization and scaling up. Other polar aprotic solvents are mild but only applicable to derived carbon nitride nanoparticles or oligomers, limiting the maximal performances.[45–47] Therefore, seeking more general solvents for pCN and deepening the understanding of the

[a]*Jiangsu Engineering Laboratory of Smart Carbon-Rich Materials and Device, Jiangsu Province Hi-Tech Key Laboratory for Bio-Medical Research, School of Chemistry and Chemical Engineering, Southeast University, Nanjing, 211189, China. E-mail: Yuanjian.Zhang@seu.edu.cn*

[b]*Medical School, Southeast University, Nanjing, 210009, China. E-mail: Yanfei.Shen@seu.edu.cn*

[c]*Institute of Industrial and Consumer Product Safety, Chinese Academy of Inspection and Quarantine, Beijing, 100176, China*

† Electronic supplementary information (ESI) available. See DOI: https://doi.org/10.1039/d3sc00642e

‡ These authors contributed equally to this work.

solubilization mechanism would be fascinating for the scalable manufacturing of molecular composites *via* industrial standard fluid-phase assembly.

Herein, we report the dissolution of pCN in mild and non-oxidizing polyphosphoric acid (PPA, pK_{a1} = 0.04–1.80, Table S1†). A multifactorial mechanism involving the cooperative absorption energy, acidity, and viscosity of solvents was discovered for the first time through comprehensive experiments and DFT calculations. This generality was further verified by the successful dissolution of pCN using more benign task-specific ionic liquids that met the above criteria. As a result, free-standing membranes consisting of pCN and carbon nanotubes (CNTs)[48–50] were prepared simply by co-dissolution, co-precipitation, and filtration. Interestingly, the pCN/CNTs membrane showed superior membrane strength compared to pristine CNTs and remarkable sterilization and wound healing effects under visible light. This work provides new insights into the development of a more universal and environmentally friendly solvent for the dissolution of pCN at the molecular level and greatly expands the prospective therapeutic applications of pCN free-standing membranes.

Results and discussion

Unlike previous super acids, PPA with variable P_2O_5 contents generally exhibited different milder acidities as well as trans-normal viscosities,[51,52] resulting in different degrees of dissolution (Fig. 1a). Among them, PPA with 75% P_2O_5 demonstrated the best solubility, leading to a clear and transparent solution (Fig. 1b and S1–3†). Moreover, PPA has almost no oxidation activity, so the potential decomposition of pCN in PPA could be avoided. To evaluate whether the structure of pCN was altered after dissolution, pCN was precipitated using methanol as a poor solvent. The recovered polymeric carbon nitride (denoted as rpCN) was still yellow (Fig. 1c inset), consistent with the original color of pCN. In contrast, oligomers of pCN (*e.g.*, melem and melam)[53,54] are usually white (Fig. S4†). Elemental analysis of pCN (Table S2†) exhibited a similar C/N mole ratio before and after dissolution, indicating that pCN was not decomposed during dissolution. Notably, although rpCN preserved the basic structure, a lighter color was observed, which was often associated with the smaller particle size and more H mass fraction with respect to pristine pCN, because of the protonation in PPA.[55]

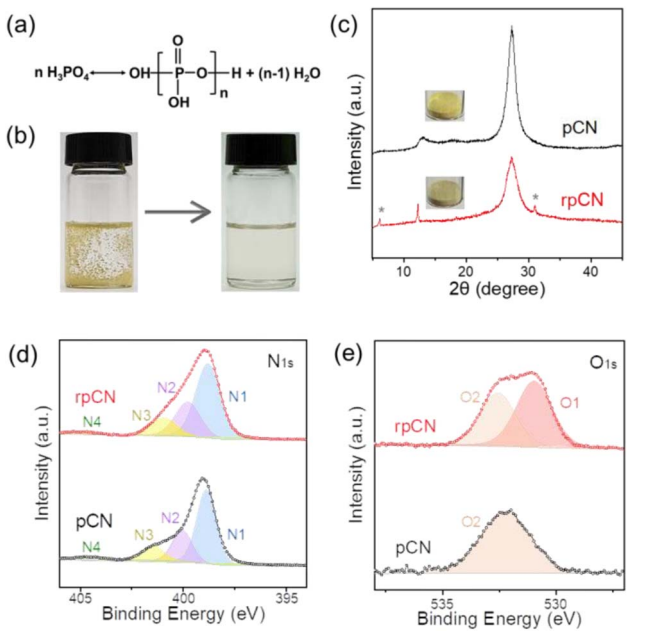

Fig. 1 (a) Equation of mutual transformation between PPA and PA. (b) Photographs of pCN dissolution in PPA. (c) XRD patterns of pristine pCN and pCN recovered from PPA (rpCN). Inset: photographs of the pCN and rpCN powders. XPS N_{1s} (d) and O_{1s} (e) spectra of pCN and rpCN.

X-ray diffraction (XRD) patterns in Fig. 1c and S5† illustrated that rpCN retained a two-dimensional layered structure for the conservation of identical 002 diffraction.[56] The slight increase in the peak width could be attributed to the disorder or expansion of the layered structure CN caused by acid intercalation, and the decrease in peak intensity was due to the reduction of plane size and periodic interlayer stacking of CN layers.[57] Fourier transform infrared (FT-IR) spectroscopy and X-ray photoelectron spectroscopy (XPS) analysis were further performed to gain an in-depth understanding of the molecular structure. For both pCN and rpCN, the characteristic FT-IR spectra (Fig. S6†) showed no obvious difference in the wavenumber ranges of 800 (tri-*s*-triazine ring out-of-plane bending), 1200–1700 (C–N aromatic heterocycle stretch vibration), and 2800–3500 (stretching vibration and hydrogen bond interaction),[58] respectively. The C_{1s} XPS spectra (Fig. S7a†) displayed the same two obvious main peaks at 288.3 eV and 284.6 eV, belonging to N–C=N of carbon nitride and impurity carbon contamination.[59] The typical components of N_{1s} spectra could be deconvoluted as four peaks in Fig. 1d, corresponding to N1 (–C=N–C, tri-*s*-triazine ring), N2 (N–$(C)_3$, bridging the N atom), N3 (C–N–H, bonded with the H atom) and N4 (charge effect),[60] respectively. The O_{1s} spectra (Fig. 1e) and P_{2p} spectra (Fig. S7b†) also confirmed the occurrence of the new P–O peak.[61]

The electronic band structures of pCN and rpCN were determined using UV-vis absorption and fluorescence spectra (Fig. S8†). The UV-vis absorption and maximum PL emission peaks were preserved, but their blue shifts were noticed due to protonation.[55] All of these results rationalized the dissolution rather than traditional degradation of pCN in PPA as judged by the color and XRD patterns, indicating that the typical molecular and electronic structure of pCN were maintained during the dissolution.

Earlier work demonstrated that protonation and intercalation reactions, resulting in sufficient electrostatic repulsion and unbundling among the pCN sheets, played an important role in dissolving pCN in concentrated sulfuric acid.[41,58] In addition, the calculated adsorption energy (E_{ads}) values for the sulfonic acid group-containing solvents supported the fact that methyl sulfonic acid was the best among them.[43] Along this line, the mechanism of pCN dissolution in PPA was further investigated. As shown in Fig. 2a, blueshifts in the optical absorption edge of the UV solid diffuse reflectance spectra of pCN indicated that the degree of protonation gradually increased during dissolution.[55] It was accompanied by a smaller 2θ value of the XRD 002 peak (Fig. S10†), indicating the possibility of PPA intercalation. More evidence of

protonation came from the numerical value of the zeta potential for the rpCN dispersion (Fig. S11†), which shifted from negative to positive surface charges in water.

Generally, the interaction between solvent molecules with a strong adsorption capacity and carbon nitride is advantageous for dissolution. For this, density functional theory (DFT) calculations were also explored.[62] As shown in Fig. 2b and S12,† the E_{ads} values of mono-polyphosphoric acid (P1, −0.79 eV) and di-polyphosphoric acid (P2, −0.88 eV) were apparently higher than that for H_2O (−0.27 eV). Comparable to methyl sulfonic acid (−0.84 eV) and concentrated sulfuric acid (−0.73 eV), PPA had an engineerable and even superior E_{ads} for the successful dissolution.[43]

Interestingly, the pCN dissolved best when the P_2O_5 content was approximately 75%. It was found that PPA with a higher content of P_2O_5 was sticky and failed to provide sufficient free protons, owing to the limited diffusion. Meanwhile, PPA with a lower P_2O_5 content was also unfavorable for dispersion (Fig. S13†). This suggested that the viscosity of PPA,[63,64] which is a generic property of polymeric materials, is also a crucial factor in the dissolution processes (Fig. 2c, S14†). It was supposed that an appropriate viscosity (700 mPa s in this work) of PPA would provide a strong shear force[65–67] at the surface of pCN during mechanical stirring to frustrate re-bundling and stimulate dissolution. In this sense, the coordinated acidity (H^+), E_{ads}, and viscosity (η) were key factors for the practically successful dissolution of pCN.

To validate the generality, ionic liquids were engineered with appropriate acidity, E_{ads}, and viscosity. It was found that the commercial compound (*i.e.*, BSO_3Py^+–$CF_3SO_3^-$) that met the above criteria could dissolve pCN well (Fig. 2d and S15†). The dissolution mechanism is summarized in Fig. 2e. The dissolution of pCN was attributed to the following factors: (1) PPA allowed E_{ads} for dissolute pCN; (2) the weak acidity of phosphoric acid protonated pCN, leading to interlayer repulsion; (3) PPA with an optimized ratio of P_2O_5 (*ca.* 75%), that is, a mixture of mono/di-phosphoric acid, had a preferred viscosity in providing shear force for delamination under mechanical agitation. Along this line, numerous solvents for pCN can be found in the future for task-specific applications, which should be regarded as a breakthrough in the development history of pCN.

The mild and effective dissolution of PPA would be beneficial for the construction of high-performance nanocomposites at the molecular level. CNTs were selected to reinforce pCN because of their excellent mechanical properties[68] and good dispersibility in PPA (Fig. S16†).[67] Fig. 3a illustrates the fabrication process of the pCN/CNTs membrane *via* facile homogeneous compounding, co-precipitation in poor solvents, and filtration. Control experiments, including those with altered ingredients (pCN and carbon nitride nanosheets), different preparation steps (with and without PPA compounding), and various solvents (PPA, HCl, H_2SO_4, MSA, and water), were also employed (Fig. S17–22†). It was found that dissolution and compounding with PPA was the key to the successful preparation of pCN/CNTs free-standing membranes.[67,69] The pCN/CNTs membrane formed by homogeneously compounding in PPA and co-precipitation was the only one that could be expediently peeled from the filtration membrane as a flat and complete surface among all fabricated samples (Fig. 3b and S19†). Notably, it displayed good flexibility and excellent tailorable properties, as it could be rolled up and cut into different shapes, and no damage was observed even when a 180° bend was performed. The thickness of the pCN/CNTs membrane could be easily regulated by changing the amount of the starting material (Fig. S23†).

The FT-IR spectra, Raman spectra, and XRD patterns of the membranes were obtained to confirm the successful

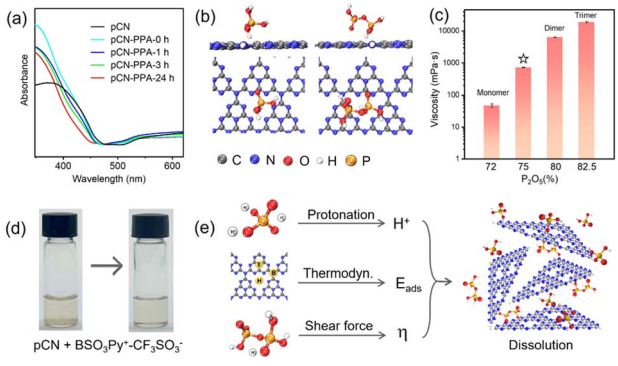

Fig. 2 (a) Solid diffuse reflectance spectra of pCN and a mixture of pCN and PPA paste (600 mg mL^{-1}, 75% P_2O_5, Fig. S9†) at different times. (b) Most stable adsorption structures of the P1 and P2 molecules on pCN obtained by DFT calculations. (c) Viscosity of PPA with different P_2O_5 contents. Star indicates the best viscosity for dissolving pCN. (d) Photographs of pCN dissolved in a task-specific ionic liquid (BSO_3Py^+–$CF_3SO_3^-$). (e) Proposed pCN dissolution mechanism.

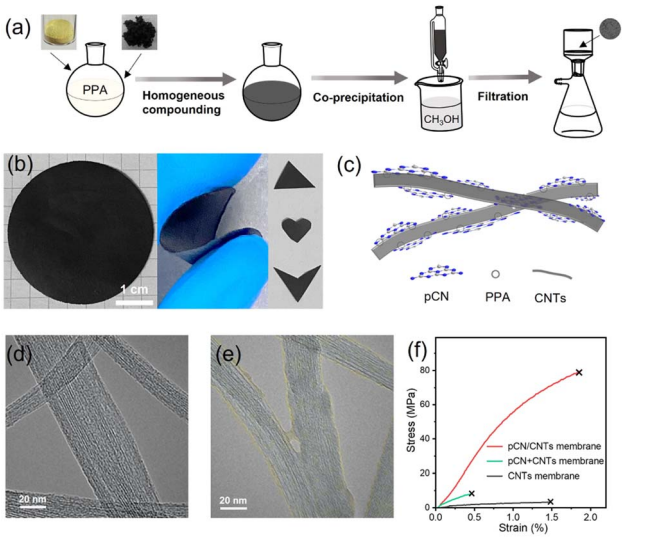

Fig. 3 (a) Fabrication process of the pCN/CNTs membrane. (b) Photographs of the as-prepared free-standing pCN/CNTs membrane, 180° folded profile, and tailored ones of different shapes. (c) Scheme of pCN and CNTs in the composite membrane. False-colored TEM images of (d) the CNTs membrane and (e) the pCN/CNTs membrane. (f) Stress–strain curves of the pCN/CNTs, pCN + CNTs, and CNTs membranes.

recombination of pCN and CNTs (Fig. S24†).[70–73] From the top surface and cross-sectional morphologies and elemental distribution (Fig. S20, 25 and 26†) measured by scanning electron microscopy (SEM) and energy dispersive X-ray spectroscopy (EDS), pCN and CNTs were distributed evenly and densely throughout the membrane. Transmission electron microscopy (TEM) images further revealed the microstructure of the CNTs before and after recombination with pCN (Fig. 3d and e). Owing to the strong π–π interfacial interactions,[74] pCN covered the surface of the CNTs bundles closely and connected them (Fig. 3c), which was expected to improve the mechanical properties. In comparison to conventional polymeric membranes, strong in-plane noncovalent bonds of the 2D-material-based membranes enhanced the mechanical strength and chemical stability, which are needed for the membrane to be utilized under harsh conditions.[75] As a result, the tensile test (Fig. 3f and S27†) showed that the ultimate strength and Young's modulus of the pCN/CNTs membrane were better than those of the control pCN + CNTs and CNTs membranes, which were filtered using pCN and/or CNTs mixtures without PPA compounding. The ratio of pCN to CNTs (5 : 1) was regarded as the optimum one in this work, and the content of pCN affected the ultimate strength and Young's modulus to some extent (Fig. S27†). Such improved mechanical properties are highly appealing for practical biomedical applications in consideration of their stability and durability.[76,77] Moreover, the homogeneous distribution of pCN on CNTs also favors maximal active site utilization in photocatalytic sterilization.

Metal-free pCN catalysts with visible light response have been widely used in environmental remediation and disinfection.[26,78,79] Unfortunately, to achieve a higher effectiveness and efficiency, three challenges remain: (i) almost all bacteria are negatively charged,[80,81] hindering the contact with the negatively charged pCN; (ii) the specific surface area of pCN powder is small, leading to fewer reactive sites; (iii) pCN catalysts are distributed unevenly in the reaction system and it is difficult to achieve a high recycling efficiency without loss. Interestingly, the as-prepared pCN/CNTs membrane well addressed these limitations and demonstrated an improved antibacterial performance. *S. aureus* and *E. coli* were used as the bacteria sources in this study, since they were represented as Gram-positive and Gram-negative bacteria, respectively.[82] The detailed processes of photocatalytic sterilization are given in Fig. S29.† As shown in Fig. 4a–c, the initial bacteria (*S. aureus* and *E. coli*) were almost completely inactivated by the pCN/CNTs membrane, from a concentration of $\sim 10^6$ CFU mL^{-1} to almost zero (0–2 CFU mL^{-1}) within 1 or 2 h. Moreover, the bacteria barely re-grew after photocatalysis (Fig. S30–32†). This performance is comparable to or even better than that of previously reported metal-modified and heterostructured pCN or other traditional catalysts (Table S3†). More importantly, after cycling more than 20 times, the integrity of the pCN/CNTs membrane evaluated by weight was still approximately 95% and maintained a high activity of up to 90% (Fig. 4d and e), revealing that it was suitable for repetitive and long-term use. In contrast, for most powdered catalysts, such as pCN powder, the mass loss after nine cycles was approximately 40% after nine cycles.

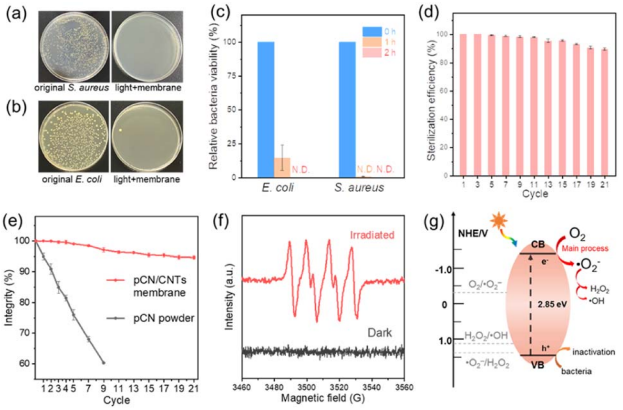

Fig. 4 Photographs of the bacterial colonies of (a) *S. aureus* and (b) *E. coli* before and after incubation with the pCN/CNTs membrane under visible light. (c) Sterilization efficiency of *E. coli* and *S. aureus* after incubation with the pCN/CNTs membrane under visible light. (d) Sterilization performance of the pCN/CNTs membrane in cycling evaluation. (e) Integrity of the pCN/CNTs membrane and pCN powder in the cycling test evaluated by weight. (f) EPR spectra of DMPO-$^{\bullet}O_2^-$ for the pCN/CNTs membrane under light irradiation and in the dark. (g) Energy band position of carbon nitride on the pCN/CNTs membrane with respect to ROS formation potential.

Given the satisfactory sterilization performance of the pCN/CNTs membrane, its photocatalytic mechanism was studied. The pCN catalyst on the membrane was evenly distributed, exposing more active sites. Upon light excitation, O_2 would be activated by reduction *via* photogenerated electrons to $^{\bullet}O_2^-$. As shown in Fig. 4f, six characteristic peaks for typical DMPO-$^{\bullet}O_2^-$ adducts were clearly observed for the irradiated pCN/CNTs membrane,[83] in contrast to the silent spectra of the unirradiated sample. In addition, according to trapping experiments (Fig. S41†) under a light source of 400 nm, the efficiency was distinctly reduced when SOD was added to the reaction solution. Moreover, the physical adsorption and photothermal effects[84] of the pCN/CNTs membrane were considered because of the large specific surface area of CNTs and the black color of the membrane. A series of control experiments (Fig. S33–42†) were also undertaken, showing that the sterilization performance originated from the generation of ROS[85] rather than any other factors. Moreover, as the water oxidation at pCN was negligible, direct attack on the bacteria at holes should also occur.[86,87] It was worth mentioning that the pCN/CNTs membrane was positively charged owing to protonation (Fig. S28†), which was helpful for disinfection performance because of the electrostatic attraction between the membrane and bacteria.

The complete photocatalytic sterilization mechanism of the pCN/CNTs membrane is shown in Fig. 4g and S43,† and the proposed elementary steps are briefly described as follows:

$$O_2 + e^- \rightarrow {}^{\bullet}O_2^- \quad (1)$$

$$^{\bullet}O_2^- + 2H^+ + e^- \rightarrow H_2O_2 \quad (2)$$

$$H_2O_2 + e^- \rightarrow {}^{\bullet}OH + OH^- \quad (3)$$

$$^{\bullet}O_2^-, H_2O_2, {}^{\bullet}OH, \text{or } h^+ + \text{bacteria} \rightarrow \text{inactivated bacteria} \quad (4)$$

As a proof of concept, we also demonstrated the potential application of pCN/CNTs membranes in practical sterilization. Some sewage samples containing *S. aureus* were collected from nature. A fully covered sandwich shelter was designed, as shown in Fig. 5a. Two layers of normal black cloth or pCN/CNTs membranes of the same size were placed on both sides and a piece of smaller white cloth was positioned between them. This cladding structure and the choice of white cloth were used to rule out the factors that accelerated the degradation of black dye under the effect of sewage and sunlight and to present vivid evidence of bacterial growth. A few days later, in a natural environment with sunlight, the white cloth encapsulated in normal cloth became yellow, indicating the growth of bacteria, whereas that in the pCN/CNTs membrane was unchanged. This clearly showed the antibacterial effect of the pCN/CNTs membrane, which suppressed the growth of bacteria under natural conditions (Fig. 5b). Inhibition zone experiments showed the same result that the pCN/CNTs membrane inhibited bacterial growth (Fig. S44†). Therefore, the pCN/CNTs membrane is expected to find practical applications in smart biomedical sterilization garments or patches.

The flexible pCN/CNTs membrane was further applied to treat *S. aureus*-infected skin wounds on laboratory mice (Fig. 5c and S45†).[88–90] The *in vitro* cytotoxicity of the pCN/CNTs membrane was firstly accessed in 4T1 cells by a 2-(2-methoxy-4-nitrophenyl)-3-(4-nitrophenyl)-5-(2,4-disulfophenyl)-2*H*-tetrazolium sodium salt (WST-8) assay.[91] As shown in Fig. 5d, no noticeable adverse effects were observed in cells after 24 h, indicating the excellent biocompatibility of the pCN/CNTs membrane. For comparison, the mice covered with the pCN/CNTs membrane and control gauze on the wounds walked together under sunlight a few times daily. The recovery of the wounds was observed, and wound size changes were tracked to evaluate the therapeutic effects (Fig. 5e, S46–S48†). It was found that *S. aureus*-infected wounds treated with the pCN/CNTs membrane under sunlight showed accelerated closure, as the wound size was smaller than that treated with the general gauze in the healing process. For an insightful understanding, H & E, Masson and CD31 staining experiments[90,92,93] (Fig. 5f) were carried out to study the inflammation response, collagen deposition and neovascularization of the wound healing effect, respectively. Compared to the control general gauze, the wounds treated with the pCN/CNTs membrane showed minor inflammatory infiltration, broader collagen disposition and more neovascularization, confirming the positive effect of the pCN/CNTs membrane on wound healing. As pCN had excellent biocompatibility, the proposed pCN/CNTs membrane is promising for biomedical applications on the body, but generally needs more strict future evaluation of safety.

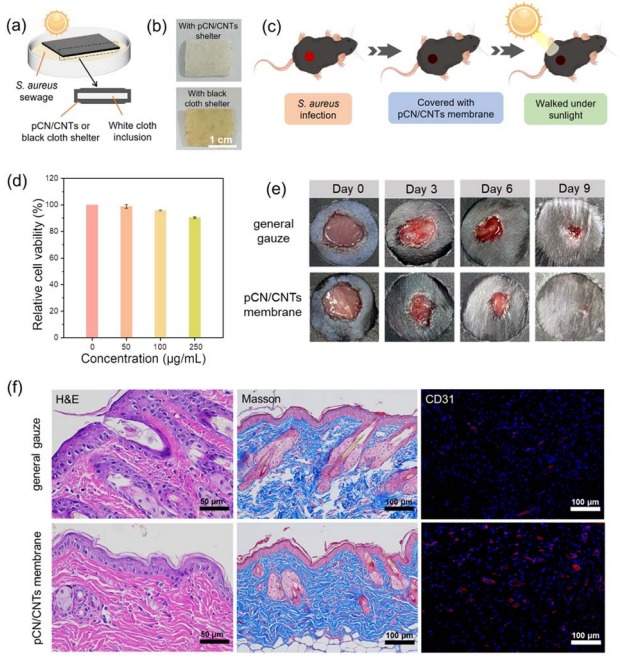

Fig. 5 (a) Sandwich structure of pCN/CNTs or control black cloth shelters and encapsulated white cloth. (b) Photographs of bacterial growth on white cloths soaked in sewage containing *S. aureus* under natural sunlight. (c) Scheme of the process of antibacterial and wound healing using the pCN/CNTs membranes for mice. (d) Biocompatibility evaluation of the pCN/CNTs membrane upon incubation with 4T1 cells by WST-8. (e) Photographs of *S. aureus*-infected wounds in laboratory mice treated with the pCN/CNTs membrane and control gauze at different times. (f) Histologic analysis (H & E, Masson, CD31) of the *S. aureus*-infected wounds after treating with the pCN/CNTs membrane and control gauze for 9 days.

Conclusions

In summary, we reported the successful dissolution of pCN in a new-generation solvent (PPA) and the associated fluid-phase assembly of a flexible pCN/CNTs membrane. Mechanism studies disclosed the crucial roles of the coordinated absorption energy, acidity and viscosity of PPA in the dissolution process. The universality of this critical finding was further supported by the discovery of more universal solvents for pCN using task-specific ionic liquids. As a result, by compounding at the molecular level, the pCN/CNTs nanocomposite membrane was fabricated *via* co-dissolution, co-precipitation, and filtration. Owing to the strong π–π interfacial interactions, pCN intimately covered the surface of the CNTs bundles and connected them into a flexible membrane with enhanced mechanical properties, which played a crucial role in further improving the durability of the membranes in long-term use. As one of the few non-powder biomedical applications, the pCN/CNTs membrane exhibited excellent photocatalytic sterilization and wound healing capacity both *in vitro* and *in vivo*. This study provides a multifactorial insight into dissolving pCN at the molecular level and a promising prospective for emergent biomedical applications using non-powdered metal-free photocatalysts in membranes.

Data availability

The data supporting the findings of this study are available within the article and in the ESI.†

Author contributions

Y. Z., X. P. and J. M. conceived and designed the experiments. X. P. performed the dissolution and mechanism studies of pCN, and the synthesis, characterization and activity evaluation of the pCN/CNTs membrane. J. M. assisted in the mechanism studies of pCN. H. Y. performed the DFT calculation. J. C. and Y. S. assisted in the wound healing for laboratory mice. J. M., Z. Z. and K. W. participated in the test of photocatalysis. G. X. assisted in the characterization of the pCN/CNTs membrane. All authors contributed to the analysis and discussion of the results. X. P., J. M. and Y. Z. co-wrote the manuscript, and Y. Z., Z. Z., R. C., S. L. and Y. S. revised the manuscript. All authors reviewed the manuscript. Y. Z. supervised the project.

Conflicts of interest

There are no conflicts to declare.

Acknowledgements

This work was supported by the National Natural Science Foundation of China (22174014 and 22074015).

Notes and references

1 F. Vatansever, W. C. de Melo, P. Avci, D. Vecchio, M. Sadasivam, A. Gupta, R. Chandran, M. Karimi, N. A. Parizotto, R. Yin, G. P. Tegos and M. R. Hamblin, Antimicrobial strategies centered around reactive oxygen species-bactericidal antibiotics, photodynamic therapy, and beyond, *FEMS Microbiol. Rev.*, 2013, **37**, 955–989.

2 B. Yang, Y. Chen and J. Shi, Reactive Oxygen Species (ROS)-Based Nanomedicine, *Chem. Rev.*, 2019, **119**, 4881–4985.

3 Y. Zhou, L. Zhang and W. Wang, Direct functionalization of methane into ethanol over copper modified polymeric carbon nitride *via* photocatalysis, *Nat. Commun.*, 2019, **10**, 506.

4 H. M. Feng, W. Wang, M. T. Zhang, S. D. Zhu, Q. Wang, J. G. Liu and S. G. Chen, 2D titanium carbide-based nanocomposites for photocatalytic bacteriostatic applications, *Appl. Catal. B*, 2020, **266**, 118609.

5 H. Sies and D. P. Jones, Reactive oxygen species (ROS) as pleiotropic physiological signalling agents, *Nat. Rev. Mol. Cell Biol.*, 2020, **21**, 363–383.

6 R. Mittler, S. I. Zandalinas, Y. Fichman and F. Van Breusegem, Reactive oxygen species signalling in plant stress responses, *Nat. Rev. Mol. Cell Biol.*, 2022, **23**, 663–679.

7 S. Cao, J. Low, J. Yu and M. Jaroniec, Polymeric photocatalysts based on graphitic carbon nitride, *Adv. Mater.*, 2015, **27**, 2150–2176.

8 Y. Nosaka and A. Y. Nosaka, Generation and Detection of Reactive Oxygen Species in Photocatalysis, *Chem. Rev.*, 2017, **117**, 11302–11336.

9 Z. Y. Teng, N. L. Yang, H. Y. Lv, S. C. Wang, M. Z. Hu, C. Y. Wang, D. Wang and G. X. Wang, Edge-Functionalized g-C_3N_4 Nanosheets as a Highly Efficient Metal-free Photocatalyst for Safe Drinking Water, *Chem*, 2019, **5**, 664–680.

10 M. Zhou, H. Ou, S. Li, X. Qin, Y. Fang, S. C. Lee, X. Wang and W. Ho, Photocatalytic Air Purification Using Functional Polymeric Carbon Nitrides, *Adv. Sci.*, 2021, **8**, 2102376.

11 J. Liu, Y. Liu, N. Liu, Y. Han, X. Zhang, H. Huang, Y. Lifshitz, S. T. Lee, J. Zhong and Z. Kang, Metal-free efficient photocatalyst for stable visible water splitting *via* a two-electron pathway, *Science*, 2015, **347**, 970–974.

12 F. K. Kessler, Y. Zheng, D. Schwarz, C. Merschjann, W. Schnick, X. Wang and M. J. Bojdys, Functional carbon nitride materials-design strategies for electrochemical devices, *Nat. Rev. Mater.*, 2017, **2**, 17030.

13 K. S. Lakhi, D. H. Park, K. Al-Bahily, W. Cha, B. Viswanathan, J. H. Choy and A. Vinu, Mesoporous carbon nitrides: synthesis, functionalization, and applications, *Chem. Soc. Rev.*, 2017, **46**, 72–101.

14 C. Tan, X. Cao, X. J. Wu, Q. He, J. Yang, X. Zhang, J. Chen, W. Zhao, S. Han, G. H. Nam, M. Sindoro and H. Zhang, Recent Advances in Ultrathin Two-Dimensional Nanomaterials, *Chem. Rev.*, 2017, **117**, 6225–6331.

15 H. Yu, R. Shi, Y. Zhao, T. Bian, Y. Zhao, C. Zhou, G. I. N. Waterhouse, L. Z. Wu, C. H. Tung and T. Zhang, Alkali-Assisted Synthesis of Nitrogen Deficient Graphitic Carbon Nitride with Tunable Band Structures for Efficient Visible-Light-Driven Hydrogen Evolution, *Adv. Mater.*, 2017, **29**, 1605148.

16 I. Ghosh, J. Khamrai, A. Savateev, N. Shlapakov, M. Antonietti and B. Konig, Organic semiconductor photocatalyst can bifunctionalize arenes and heteroarenes, *Science*, 2019, **365**, 360–366.

17 N. Karjule, C. Singh, J. Barrio, J. Tzadikov, I. Liberman, M. Volokh, E. Palomares, I. Hod and M. Shalom, Carbon Nitride-Based Photoanode with Enhanced Photostability and Water Oxidation Kinetics, *Adv. Funct. Mater.*, 2021, **31**, 2101724.

18 Z. Teng, Q. Zhang, H. Yang, K. Kato, W. Yang, Y.-R. Lu, S. Liu, C. Wang, A. Yamakata, C. Su, B. Liu and T. Ohno, Atomically dispersed antimony on carbon nitride for the artificial photosynthesis of hydrogen peroxide, *Nat. Catal.*, 2021, **4**, 374–384.

19 S. Mazzanti, G. Manfredi, A. J. Barker, M. Antonietti, A. Savateev and P. Giusto, Carbon Nitride Thin Films as All-In-One Technology for Photocatalysis, *ACS.Catal.*, 2021, **11**, 11109–11116.

20 J. Li, K. Zhang, Y. Zhao, C. Wang, L. Wang, L. Wang, M. Liao, L. Ye, Y. Zhang, Y. Gao, B. Wang and H. Peng, High-Efficiency and Stable Li-CO_2 Battery Enabled by Carbon Nanotube/Carbon Nitride Heterostructured Photocathode, *Angew. Chem., Int. Ed.*, 2022, **61**, e202114612.

21 N. Rohaizad, C. C. Mayorga-Martinez, M. Fojtu, N. M. Latiff and M. Pumera, Two-dimensional materials in biomedical, biosensing and sensing applications, *Chem. Soc. Rev.*, 2021, **50**, 619–657.

22 M. Kou, Y. Wang, Y. Xu, L. Ye, Y. Huang, B. Jia, H. Li, J. Ren, Y. Deng, J. Chen, Y. Zhou, K. Lei, L. Wang, W. Liu, H. Huang and T. Ma, Molecularly Engineered Covalent Organic

Frameworks for Hydrogen Peroxide Photosynthesis, *Angew. Chem., Int. Ed.*, 2022, **61**, e202200413.

23 R. Kuriki, K. Sekizawa, O. Ishitani and K. Maeda, Visible-light-driven CO_2 reduction with carbon nitride: enhancing the activity of ruthenium catalysts, *Angew. Chem., Int. Ed.*, 2015, **54**, 2406–2409.

24 L. H. Lin, Z. Y. Lin, J. Zhang, X. Cai, W. Lin, Z. Y. Yu and X. C. Wang, Molecular-level insights on the reactive facet of carbon nitride single crystals photocatalysing overall water splitting, *Nat. Catal.*, 2020, **3**, 649–655.

25 D. M. Zhao, Y. Q. Wang, C. L. Dong, Y. C. Huang, J. Chen, F. Xue, S. H. Shen and L. J. Guo, Boron-doped nitrogen-deficient carbon nitride-based Z-scheme heterostructures for photocatalytic overall water splitting, *Nat. Energy*, 2021, **6**, 388–397.

26 W. J. Ong, L. L. Tan, Y. H. Ng, S. T. Yong and S. P. Chai, Graphitic Carbon Nitride (g-C_3N_4)-Based Photocatalysts for Artificial Photosynthesis and Environmental Remediation: Are We a Step Closer To Achieving Sustainability?, *Chem. Rev.*, 2016, **116**, 7159–7329.

27 P. Xia, S. Cao, B. Zhu, M. Liu, M. Shi, J. Yu and Y. Zhang, Designing a 0D/2D S-Scheme Heterojunction over Polymeric Carbon Nitride for Visible-Light Photocatalytic Inactivation of Bacteria, *Angew. Chem., Int. Ed.*, 2020, **59**, 5218–5225.

28 T. Banerjee, F. Podjaski, J. Kroger, B. P. Biswal and B. V. Lotsch, Polymer photocatalysts for solar-to-chemical energy conversion, *Nat. Rev. Mater.*, 2021, **6**, 168–190.

29 Z. Zhou, Y. Zhang, Y. Shen, S. Liu and Y. Zhang, Molecular engineering of polymeric carbon nitride: advancing applications from photocatalysis to biosensing and more, *Chem. Soc. Rev.*, 2018, **47**, 2298–2321.

30 J. Xu, T. J. Brenner, L. Chabanne, D. Neher, M. Antonietti and M. Shalom, Liquid-based growth of polymeric carbon nitride layers and their use in a mesostructured polymer solar cell with V(oc) exceeding 1 V, *J. Am. Chem. Soc.*, 2014, **136**, 13486–13489.

31 J. Xu and M. Antonietti, The Performance of Nanoparticulate Graphitic Carbon Nitride as an Amphiphile, *J. Am. Chem. Soc.*, 2017, **139**, 6026–6029.

32 I. Krivtsov, D. Mitoraj, C. Adler, M. Ilkaeva, M. Sardo, L. Mafra, C. Neumann, A. Turchanin, C. Li, B. Dietzek, R. Leiter, J. Biskupek, U. Kaiser, C. Im, B. Kirchhoff, T. Jacob and R. Beranek, Water-Soluble Polymeric Carbon Nitride Colloidal Nanoparticles for Highly Selective Quasi-Homogeneous Photocatalysis, *Angew. Chem., Int. Ed.*, 2020, **59**, 487–495.

33 C. Jia, L. Yang, Y. Zhang, X. Zhang, K. Xiao, J. Xu and J. Liu, Graphitic Carbon Nitride Films: Emerging Paradigm for Versatile Applications, *ACS Appl. Mater. Interfaces*, 2020, **12**, 53571–53591.

34 X. Zhang, X. Xie, H. Wang, J. Zhang, B. Pan and Y. Xie, Enhanced photoresponsive ultrathin graphitic-phase C_3N_4 nanosheets for bioimaging, *J. Am. Chem. Soc.*, 2013, **135**, 18–21.

35 J. Zhang, M. Zhang, L. Lin and X. Wang, Sol processing of conjugated carbon nitride powders for thin-film fabrication, *Angew. Chem., Int. Ed.*, 2015, **54**, 6297–6301.

36 B. Kumru, M. Shalom, M. Antonietti and B. V. K. J. Schmidt, Reinforced Hydrogels *via* Carbon Nitride Initiated Polymerization, *Macromolecules*, 2017, **50**, 1862–1869.

37 P. Hu, C. J. Chen, R. Zeng, J. W. Xiang, Y. Huang, D. F. Hou, Q. Li and Y. H. Huang, Facile synthesis of bimodal porous graphitic carbon nitride nanosheets as efficient photocatalysts for hydrogen evolution, *Nano Energy*, 2018, **50**, 376–382.

38 Y. Wang, N. Wu, Y. Wang, H. Ma, J. Zhang, L. Xu, M. K. Albolkany and B. Liu, Graphite phase carbon nitride based membrane for selective permeation, *Nat. Commun.*, 2019, **10**, 2500.

39 Q. Cao, B. Kumru, M. Antonietti and B. V. K. J. Schmidt, Graphitic carbon nitride and polymers: a mutual combination for advanced properties, *Mater. Horiz.*, 2020, **7**, 762–786.

40 w. wenbo, W. Dong, L. Ji, Y. Xia and S. Yang, Solubility of graphene-like two-dimensional layered C_3N_3, *Chem. Commun.*, 2022, **58**, 13971–13974.

41 Z. Zhou, J. Wang, J. Yu, Y. Shen, Y. Li, A. Liu, S. Liu and Y. Zhang, Dissolution and liquid crystals phase of 2D polymeric carbon nitride, *J. Am. Chem. Soc.*, 2015, **137**, 2179–2182.

42 J. Y. Song, H. J. Kang, J. C. Won, Y. H. Kim, Y. S. Jun and H. S. Jeong, The true liquid crystal phases of 2D polymeric carbon nitride and macroscopic assembled fibers, *Mater. Horiz.*, 2019, **6**, 1726–1732.

43 C. Huang, J. Wen, Y. Shen, F. He, L. Mi, Z. Gan, J. Ma, S. Liu, H. Ma and Y. Zhang, Dissolution and homogeneous photocatalysis of polymeric carbon nitride, *Chem. Sci.*, 2018, **9**, 7912–7915.

44 T. S. Miller, T. M. Suter, A. M. Telford, L. Picco, O. D. Payton, F. Russell-Pavier, P. L. Cullen, A. Sella, M. S. P. Shaffer, J. Nelson, V. Tileli, P. F. McMillan and C. A. Howard, Single Crystal, Luminescent Carbon Nitride Nanosheets Formed by Spontaneous Dissolution, *Nano Lett.*, 2017, **17**, 5891–5896.

45 Y. Xu, M. Fan, W. Yang, Y. Xiao, L. Zeng, X. Wu, Q. Xu, C. Su and Q. He, Homogeneous Carbon/Potassium-Incorporation Strategy for Synthesizing Red Polymeric Carbon Nitride Capable of Near-Infrared Photocatalytic H_2 Production, *Adv. Mater.*, 2021, **33**, e2101455.

46 D. Burmeister, H. A. Tran, J. Muller, M. Guerrini, C. Cocchi, J. Plaickner, Z. Kochovski, E. J. W. List-Kratochvil and M. J. Bojdys, Optimized Synthesis of Solution-Processable Crystalline Poly(Triazine Imide) with Minimized Defects for OLED Application, *Angew. Chem., Int. Ed.*, 2022, **61**, e202111749.

47 Y. F. Fang, Y. H. Hou, H. Yang, R. Chen, W. Li, J. Ma, D. Han, X. W. Cao, S. Q. Liu, Y. F. Shen and Y. J. Zhang, Elucidating Orbital Delocalization Effects on Boosting Electrochemiluminescence Efficiency of Carbon Nitrides, *Adv. Opt. Mater.*, 2022, **10**, 2201017.

48 Z. Wu, Z. Chen, X. Du, J. M. Logan, J. Sippel, M. Nikolou, K. Kamaras, J. R. Reynolds, D. B. Tanner, A. F. Hebard and A. G. Rinzler, Transparent, conductive carbon nanotube films, *Science*, 2004, **305**, 1273–1276.

49 V. A. Davis, A. N. Parra-Vasquez, M. J. Green, P. K. Rai, N. Behabtu, V. Prieto, R. D. Booker, J. Schmidt, E. Kesselman, W. Zhou, H. Fan, W. W. Adams, R. H. Hauge, J. E. Fischer, Y. Cohen, Y. Talmon, R. E. Smalley and M. Pasquali, True solutions of single-walled carbon nanotubes for assembly into macroscopic materials, *Nat. Nanotechnol.*, 2009, **4**, 830–834.

50 V. Schroeder, S. Savagatrup, M. He, S. Lin and T. M. Swager, Carbon Nanotube Chemical Sensors, *Chem. Rev.*, 2019, **119**, 599–663.

51 F. D. Popp and W. E. McEwen, Polyphosphoric Acids As A Reagent In Organic Chemistry, *Chem. Rev.*, 1958, **58**, 321–401.

52 I. S. Skorynina, S. S. Gusev, N. K. Vorob'yeva and I. N. Yermolenko, Phosphorylation of cellulose by polyphosphoric acids, *Polym. Sci.*, 1970, **12**, 2778–2785.

53 C. E. Redemann and H. J. Lucas, Some Derivatives of Cyameluric Acid and Probable Structures of Melam, Melem and Melon, *J. Am. Chem. Soc.*, 1940, **62**, 842–846.

54 B. Jurgens, E. Irran, J. Senker, P. Kroll, H. Muller and W. Schnick, Melem (2,5,8-triamino-tri-s-triazine), an important intermediate during condensation of melamine rings to graphitic carbon nitride: synthesis, structure determination by X-ray powder diffractometry, solid-state NMR, and theoretical studies, *J. Am. Chem. Soc.*, 2003, **125**, 10288–10300.

55 Y. Zhang, A. Thomas, M. Antonietti and X. Wang, Activation of carbon nitride solids by protonation: morphology changes, enhanced ionic conductivity, and photoconduction experiments, *J. Am. Chem. Soc.*, 2009, **131**, 50–51.

56 P. Zhang, D. Sun, A. Cho, S. Weon, S. Lee, J. Lee, J. W. Han, D. P. Kim and W. Choi, Modified carbon nitride nanozyme as bifunctional glucose oxidase-peroxidase for metal-free bioinspired cascade photocatalysis, *Nat. Commun.*, 2019, **10**, 940.

57 A. M. Dimiev, S. M. Bachilo, R. Saito and J. M. Tour, Reversible formation of ammonium persulfate/sulfuric acid graphite intercalation compounds and their peculiar Raman spectra, *ACS Nano*, 2012, **6**, 7842–7849.

58 S. Yang, Y. Gong, J. Zhang, L. Zhan, L. Ma, Z. Fang, R. Vajtai, X. Wang and P. M. Ajayan, Exfoliated graphitic carbon nitride nanosheets as efficient catalysts for hydrogen evolution under visible light, *Adv. Mater.*, 2013, **25**, 2452–2456.

59 Z. Lin and X. Wang, Nanostructure engineering and doping of conjugated carbon nitride semiconductors for hydrogen photosynthesis, *Angew. Chem., Int. Ed.*, 2013, **52**, 1735–1738.

60 W. Wu, J. Zhang, W. Fan, Z. Li, L. Wang, X. Li, Y. Wang, R. Wang, J. Zheng, M. Wu and H. Zeng, Remedying Defects in Carbon Nitride To Improve both Photooxidation and H_2 Generation Efficiencies, *ACS.Catal.*, 2016, **6**, 3365–3371.

61 J. Wu, S. Yang, J. Li, Y. Yang, G. Wang, X. Bu, P. He, J. Sun, J. Yang, Y. Deng, G. Ding and X. Xie, Electron Injection of Phosphorus Doped g-C_3N_4 Quantum Dots: Controllable Photoluminescence Emission Wavelength in the Whole Visible Light Range with High Quantum Yield, *Adv. Opt. Mater.*, 2016, **4**, 2095–2101.

62 B. C. Zhu, L. Y. Zhang, B. Cheng and J. G. Yu, First-principle calculation study of tri-s-triazine-based g-C_3N_4: A review, *Appl. Catal. B*, 2018, **224**, 983–999.

63 T. G. Hiss and E. L. Cussler, Diffusion in High-Viscosity Liquids, *AICHE J.*, 1973, **19**, 698–703.

64 J. B. Baek, C. B. Lyons and L. S. Tan, Grafting of vapor-grown carbon nanofibers *via in situ* polycondensation of 3-phenoxybenzoic acid in poly(phosphoric acid), *Macromolecules*, 2004, **37**, 8278–8285.

65 S. W. Han, S. J. Oh, L. S. Tan and J. B. Baek, One-pot purification and functionalization of single-walled carbon nanotubes in less-corrosive poly(phosphoric acid), *Carbon*, 2008, **46**, 1841–1849.

66 D. C. Yue, T. B. Ma, Y. Z. Hu, J. Yeon, A. C. T. van Duin, H. Wang and J. B. Luo, Tribochemistry of Phosphoric Acid Sheared between Quartz Surfaces: A Reactive Molecular Dynamics Study, *J. Phys. Chem. C*, 2013, **117**, 25604–25614.

67 J. M. Seo, L. S. Tan and J. B. Baek, Defect/Edge-Selective Functionalization of Carbon Materials by "Direct" Friedel-Crafts Acylation Reaction, *Adv. Mater.*, 2017, **29**, 1606317.

68 R. H. Baughman, Materials Science: Putting a New Spin on Carbon Nanotubes, *Science*, 2000, **290**, 1310–1311.

69 T. E. Helminiak and R. C. Evers, *Polymers for Fibers and Elastomers*, 1984, pp. 415–420, DOI: **10.1021/bk-1984-0260.ch026**.

70 N. A. Kumar, I. Y. Jeon, G. J. Sohn, R. Jain, S. Kumar and J. B. Baek, Highly conducting and flexible few-walled carbon nanotube thin film, *ACS Nano*, 2011, **5**, 2324–2331.

71 I. A. Kinloch, J. Suhr, J. Lou, R. J. Young and P. M. Ajayan, Composites with carbon nanotubes and graphene: An outlook, *Science*, 2018, **362**, 547–553.

72 Y. A. Liu, Y. L. Su, J. Y. Guan, J. L. Cao, R. N. Zhang, M. R. He, K. Gao, L. J. Zhou and Z. Y. Jiang, 2D Heterostructure Membranes with Sunlight-Driven Self-Cleaning Ability for Highly Efficient Oil-Water Separation, *Adv. Funct. Mater.*, 2018, **28**, 1706545.

73 V. Negri, J. Pacheco-Torres, D. Calle and P. Lopez-Larrubia, Carbon Nanotubes in Biomedicine, *Top. Curr. Chem.*, 2020, **378**, 15.

74 Y. Y. Zhang, Y. X. Song, Y. F. Shen, K. Y. Chen, Q. Zhou, Y. Q. Lv, H. Yang, E. S. Xu, S. Q. Liu, L. Liu and Y. J. Zhang, Water Molecule-Triggered Anisotropic Deformation of Carbon Nitride Nanoribbons Enabling Contactless Respiratory Inspection, *CCS Chem.*, 2021, **3**, 1615–1625.

75 Z. Chen, Y. Lan, Y. Hong and W. G. Lan, Review of 2D Graphitic Carbon Nitride-Based Membranes: Principles, Syntheses, and Applications, *ACS Appl. Nano Mater.*, 2022, **5**, 12343–12365.

76 M. Chao, L. He, M. Gong, N. Li, X. Li, L. Peng, F. Shi, L. Zhang and P. Wan, Breathable $Ti_3C_2T_x$ MXene/Protein

Nanocomposites for Ultrasensitive Medical Pressure Sensor with Degradability in Solvents, *ACS Nano*, 2021, **15**, 9746–9758.

77 B. Yang, J. Kong and X. Fang, Programmable CRISPR-Cas9 microneedle patch for long-term capture and real-time monitoring of universal cell-free DNA, *Nat. Commun.*, 2022, **13**, 3999.

78 W. Wang, C. Zhou, Y. Yang, G. Zeng, C. Zhang, Y. Zhou, J. Yang, D. Huang, H. Wang, W. Xiong, X. Li, Y. Fu, Z. Wang, Q. He, M. Jia and H. Luo, Carbon nitride based photocatalysts for solar photocatalytic disinfection, can we go further?, *Chem. Eng. J.*, 2021, **404**, 126540.

79 X. Yang, Y. Ye, J. Sun, Z. Li, J. Ping and X. Sun, Recent Advances in g-C_3N_4 -Based Photocatalysts for Pollutant Degradation and Bacterial Disinfection: Design Strategies, Mechanisms, and Applications, *Small*, 2022, **18**, e2105089.

80 X. K. Zeng, Y. Liu, Y. Xia, M. H. Uddin, D. H. Xia, D. T. McCarthy, A. Deletic, J. G. Yu and X. W. Zhang, Cooperatively modulating reactive oxygen species generation and bacteria-photocatalyst contact over graphitic carbon nitride by polyethylenimine for rapid water disinfection, *Appl. Catal. B*, 2020, **274**, 119095.

81 L. Huang, S. Xu, Z. Wang, K. Xue, J. Su, Y. Song, S. Chen, C. Zhu, B. Z. Tang and R. Ye, Self-Reporting and Photothermally Enhanced Rapid Bacterial Killing on a Laser-Induced Graphene Mask, *ACS Nano*, 2020, **14**, 12045–12053.

82 J. Jin, J. Mao, W. Wu, Y. Jiang, W. Ma, P. Yu and L. Mao, Highly Efficient Electrosynthesis of Nitric Oxide for Biomedical Applications, *Angew. Chem., Int. Ed.*, 2022, **61**, e202210980.

83 P. Li, J. Li, X. Feng, J. Li, Y. Hao, J. Zhang, H. Wang, A. Yin, J. Zhou, X. Ma and B. Wang, Metal-organic frameworks with photocatalytic bactericidal activity for integrated air cleaning, *Nat. Commun.*, 2019, **10**, 2177.

84 Z. S. Wang, H. J. Yu, Y. F. Xiao, L. Zhang, L. M. Guo, L. X. Zhang and X. P. Dong, Free-standing composite films of multiple 2D nanosheets: Synergetic photothermocatalysis/photocatalysis for efficient removal of formaldehyde under ambient condition, *Chem. Eng. J.*, 2020, **394**, 125014.

85 B. Ran, Z. Wang, W. Cai, L. Ran, W. Xia, W. Liu and X. Peng, Organic Photo-antimicrobials: Principles, Molecule Design, and Applications, *J. Am. Chem. Soc.*, 2021, **143**, 17891–17909.

86 Y. Hou, X. Li, Q. Zhao, G. Chen and C. L. Raston, Role of hydroxyl radicals and mechanism of Escherichia coli inactivation on Ag/AgBr/TiO_2 nanotube array electrode under visible light irradiation, *Environ. Sci. Technol.*, 2012, **46**, 4042–4050.

87 Z. Qi, G. Li, M. Wang, C. Chen, Z. Xu and T. An, Photoelectrocatalytic inactivation mechanism of E. coli DH5α (TET) and synergistic degradation of corresponding antibiotics in water, *Water Res.*, 2022, **215**, 118240.

88 H. Sun, N. Gao, K. Dong, J. Ren and X. Qu, Graphene quantum dots-band-aids used for wound disinfection, *ACS Nano*, 2014, **8**, 6202–6210.

89 X. Lin, Y. Fang, Z. Hao, H. Wu, M. Zhao, S. Wang and Y. Liu, Bacteria-Triggered Multifunctional Hydrogel for Localized Chemodynamic and Low-Temperature Photothermal Sterilization, *Small*, 2021, **17**, e2103303.

90 L. Wang, Q. Su, Y. Liu, T. Yimamumaimaiti, D. Hu, J. J. Zhu and J. R. Zhang, A self-powered and drug-free diabetic wound healing patch breaking hyperglycemia and low H_2O_2 limitations and precisely sterilizing driven by electricity, *Chem. Sci.*, 2022, **13**, 12136–12143.

91 J. Ma, X. Peng, Z. Zhou, H. Yang, K. Wu, Z. Fang, D. Han, Y. Fang, S. Liu, Y. Shen and Y. Zhang, Extended Conjugation Tuning Carbon Nitride for Non-sacrificial H_2O_2 Photosynthesis and Hypoxic Tumor Therapy, *Angew. Chem., Int. Ed.*, 2022, **61**, e202210856.

92 M. Kharaziha, A. Baidya and N. Annabi, Rational Design of Immunomodulatory Hydrogels for Chronic Wound Healing, *Adv. Mater.*, 2021, **33**, e2100176.

93 R. Huang, X. Zhang, W. Li, L. Shang, H. Wang and Y. Zhao, Suction Cups-Inspired Adhesive Patch with Tailorable Patterns for Versatile Wound Healing, *Adv. Sci.*, 2021, **8**, e2100201.